DOI 10.5012/bkcs.2010.31.11.3093

Suppression of Charge Recombination Rate in Nanocrystalline SnO_2 by Thin Coatings of Divalent Oxides in Dye-Sensitized Solar Cells†

Chaehyeon Lee,[‡,§] Gi-Won Lee,[‡] Weekyung Kang,[§] Doh-Kwon Lee,[‡] Min Jae Ko,[‡] Kyoungkon Kim,[‡] and Nam-Gyu Park[#,*]

[‡]*Solar Cell Center, Korea Institute of Science and Technology, Seoul 136-791, Korea*
[§]*Department of Chemistry, Soongsil University, Seoul 156-743, Korea*
[#]*School of Chemical Engineering, Sungkyunkwan University, Suwon 440-746, Korea. [*]E-mail: npark@skku.edu*
Received April 26, 2010, Accepted May 26, 2010

The core-shell SnO_2@AO (A = Ni, Cu, Zn and Mg) films were prepared and the effects of coatings on photovoltaic properties were investigated. Studies on X-ray photoelectron spectroscopy, energy dispersive X-ray analysis and transmission electron microscopy showed the formation of divalent oxides on the surface of SnO_2 nanoparticles. It was commonly observed that all the dye-sensitized core-shell films exhibited higher photovoltage than the bare SnO_2 film. Transient photovoltage measurements confirmed that the improved photovoltages were related to the decreased time constants for electron recombination.

Key Words: Core-shell, Surface coating, Dye-sensitized solar cell, Charge recombination, Nanocrystalline SnO_2

Introduction

Dye-sensitized solar cell (DSSC) has received a great attention over two decades and as a result energy conversion efficiency as high as 11% has been achieved.[1-3] DSSC is mainly composed of a wide band-gap semiconductor, a dye and a redox-type electrolyte. Since semiconductor layer is usually made of nanocrystalline mesoporous structure, a lot of semiconductor/dye/electrolyte interfaces form compared with solid/solid p-n junction type solar cell. At the interface, photo-injected electrons can be recombined with oxidized dyes *via* surface state of nanocrystalline semiconductor, which is likely to occur at open-circuit condition. Such a recombination affects open-circuit photovoltage by changing the Fermi energy level. Therefore, a modification of nanocrystalline surface is important research field in DSSC, in terms of interfacial recombination control.

Kay and Grätzel[4] reported that modification of nanocrystalline SnO_2 surface with a few angstrom-thick insulating material improved significantly photovoltage along with an increase in photocurrent and, in the case of TiO_2, however, its surface modification with very thin insulating materials improved photovoltage but diminished photocurrent. Park *et al*.[5] reported the similar results, where surface modification of nanocrystalline SnO_2 and TiO_2 with a few angstrom-thick zinc oxide, which was confirmed by EXAFS analysis, increased photovoltage. Zaban group[6] studied with a SnO_2 film whose surface was coated with thin TiO_2 layer, in which the improved photovoltage and photocurrent by surface modification were analyzed by difference in conduction band energy between the core SnO_2 and the shell TiO_2. One year after, the same research group reported on a nanoporous TiO_2 electrode coated with a thin $SrTiO_3$ layer, where the increased photovoltage and decreased photocurrent were due to the fact that the $SrTiO_3$ layer shifted the conduction band of the TiO_2 in the negative direction as a consequence of surface dipole generated at the $TiO_2/SrTiO_3$ interface, rather than energy barrier. The surface dipole was explained by the difference in either the electron affinity or isoelectric point of two semiconductors.[7] In the case of using TiO_2 as a core material, the change in photovoltage by shell coatings was reported to be more closely related with difference in the isoelectric point than the electron affinity of the two materials at the core-shell interface.[8] Meanwhile, Tennakone group[9] reported that the improved photovoltage by coating the very thin oxide layer on the surface of nanocrystalline SnO_2 was because the shell layer acted as a barrier layer against recombination due to higher conduction band edge of shell material. According to the reports on core-shell materials in DSSC, surface shell coatings seem most likely to lead to an increase in photovoltage. Although the assessments for the improved photovoltage seem to be valid, there is still argument on the basis for the improved photovoltage. Therefore, we have been interested in investigating electron transfer at SnO_2/electrolyte before and after surface coatings, where conduction band edges of the shell materials are higher or lower than that of the core SnO_2 but all of the shell materials have lower electron affinities.

We report here that photovoltaic property on DSSC based on nanocryatlline SnO_2 whose surface was modified with Ni, Cu, Zn and Mg oxide materials. It has been known that conduction band edges of NiO, CuO, ZnO and MgO are different in the bulk solid state, while their electron affinities are similar. The surface coating layers were investigated using TEM, EDX and XPS. Effects of shell coatings on photocurrent-voltage, external quantum efficiency, transport and recombination of photo-injected electrons and interfacial impedance were studied.

Experimental Section

Preparation of nanocrystalline SnO_2 films. SnO_2 paste was synthesized as follows. Ethyl cellulose (Aldirich), lauric acid (Fluka) and terpineol (Fluka) were added into the ethanol solu-

†This paper is dedicated to Professor Hasuck Kim for his outstanding contribution to electrochemistry and analytical chemistry.

tion of SnO_2 particles (average particle diameter of about 26 nm, NanoTek, Japan) which were dispersed using an Ultra Apex Mill (Model UAM-015, Kotobuki) at 30 Hz for 90 min, and then ethanol was removed from the solution using a rotary evaporator to obtain viscous pastes. The nominal weight ratio of SnO_2/terpineol/ethylcellulose/lauric acid was about 1/4/0.3/0.1. The mesoporous SnO_2 film was fabricated on a transparent conducting glass substrate (FTO glass, Pilkington, TEC-8, 8 Ω/sq, 2.3 mm thick) using doctor blade technique. The SnO_2 films were heated at 500 °C for 30 min. The thicknesses of bare SnO_2 films used for this study were about 6 μm as measured by Alpha-Step IQ surface profiler (KLA Tencor).

Shell coatings and DSSC fabrication. The shell coatings were preformed by dipping of the annealed SnO_2 electrode in 20 mM aqueous solution containing a metal acetate precursor of Ni $(CH_3CO_2)_2{\cdot}4H_2O$, Cu $(CH_3CO_2)_2{\cdot}H_2O$, Zn $(CH_3CO_2)_2{\cdot}2H_2O$ and Mg $(CH_3CO_2)_2{\cdot}4H_2O$ for preparing NiO, Cuo, ZnO and MgO shells, respectively, for 5 h at 50 °C, followed by washing with water for 20 s and then heating at 500 °C for 30 min. After the cooling to 80 °C, the bare SnO_2 and the AO-coated SnO_2 films were sensitized with 0.5 mM Ru[L_2(NCS)$_2$] (L = 2,2'-bipyridyl-4,4'-dicarboxylic acid, N3, Solaronix) ethanol solution at ambient temperature for 48 h. A Pt counter electrode was prepared by coating a 0.7 mM H_2PtCl_6 isopropanol solution on a FTO glass, followed by heating at 400 °C for 20 min. The two electrodes were assembled using 25 μm-thick surlyn (Dupont 1702). An electrolyte solution was composed of 0.7 M 1-propyl-3-methylimidazolium iodide (PMII), 0.03 M I_2, 0.05 M guanidinium thiocyanate (GSCN) and 0.5 M 4-tert-butylpyridine (TBP) in acetonitrile and valeronitrile (85:15 v/v). Active area of dye-coated SnO_2 film was about 0.25 cm^2, which was measured by an image analysis program equipped with a digital microscope camera (Moticam 1000).

Characterizations. The shell coatings were investigated by transmission electron microscopy (TEM, Philips CM30, operation at 200 kV), energy dispersive X-ray analysis (EDX) and X-ray photoelectron spectroscopy (XPS). XPS spectra were recorded using a Perkin-Elmer PHI 5800 ESCA system with standard Al-Kα source (1486.6 eV) working at 250 W. The calibration of binding energy scale was performed with the C 1s line (284.8 eV) from the carbon contamination layer. Photocurrent-voltage measurements were performed using a Keithley model 2400 source measuring unit. A 1000 W Xenon lamp (Spectra-Physics) served as a light source and its light intensity was adjusted using a NREL-calibrated Si solar cell equipped with a KG-2 filter for approximating AM 1.5G one sun light intensity. During photocurrent-voltage measurement, DSSC was covered with a black mask with an aperture to avoid additional light coming through lateral space.[10,11] UV-vis absorption spectra of the dye-adsorbed films were measured with UV-vis spectrophotometer (Agilent 8453). IPCE was measured as a function of wavelength from 300 nm to 800 nm using a specially designed IPCE system for dye-sensitized solar cell (PV Measurements, Inc.). A 75 W Xenon lamp was used as a light source for generating monochromatic beam. Calibration was performed using a silicon photodiode, which was calibrated using the NIST-calibrated photodiode G425 as a standard, and IPCE values were collected at a low chopping speed of 10 Hz.

Photocurrent and photovoltage transient measurements. Charge collection time was measured using photocurrent transient induced by small-intensity laser pulse superimposed on bias light. The cells were probed with a weak laser pulse at 532 nm superimposed on a relatively large, back ground (bias) illumination at 680 nm.[12,13] The bias light was illuminated by a 0.5 W diode laser (B&W TEK Inc., Model: BWF1-670-300E/55370). The intensity of the bias light was adjusted using ND filters (neutral density filters). The 680 nm bias light is only weakly absorbed by the dye, and therefore the injected electrons are introduced into a narrow spatial region of the film, corresponding to where the probe light enters the film. A 30 mW frequency-doubled Nd:YAG laser (Laser-Export Co. Ltd. Model: LCS-DTL-314QT) (λ = 532 nm, pulse duration 10 ns) was used as probe light. The photocurrent transients were obtained by using a Stanford Research Systems model SR570 low-noise current preamplifier, amplified by a Stanford Research Systems model SR560 low-noise preamplifier, and recorded on Tektronics TDS 3054B digital phosphore oscilloscope 500MHz 5GS/s DPO. The photovoltage transient were obtained by using a Stanford Research System model SR570 low-noise preamplifier, and then recorded on Tektronics TDS 3054B digital phosphore oscilloscope 500 MHz 5 GS/s DPO. The response time of the preamplifier at the range of photocurrent and photovoltages used was less than 1 ms. The light intensity of the probe light was adjusted so that the collected charge due to the transient photocurrent and photovoltage were less than 1% of the steady-state charge as estimated from the product of the steady-state short-circuit photocurrent/voltage, the time constant for electron collection, and the time of electron life time.

Results and Discussion

Figure 1 shows TEM micrographs of SnO_2 particles treated with metal acetates and annealed at air atmosphere. Except for the copper acetate coating on SnO_2, it is difficult to recognize the shell coatings from TEM images. However, EDX analysis confirms the presence of each element having the atomic percent ranging from 1 to 4%, which underlines that surface coating materials form very thin layers on the SnO_2 surface. Copper acetate coating, on the other hand, leads to a relatively thick layer. In order to investigate valence states of the surface coating elements, XPS study was conducted.

Figure 2 shows Ni 2p, Cu 2p, Zn 2p and Mg 1s XPS spectra. The Ni $2p_{3/2}$ and $2p_{1/2}$ peak positions observed for the SnO_2 film treated with nickel acetate are 855.9 eV and 874.4 eV, respectively, with the shake-up satellite peak at 861.8 eV. The crystalline NiO was reported to show usually the Ni $2p_{3/2}$ peak position at 853.3 - 854.6 eV with multiplet splitting at 856.1 eV and shake-up satellite at 861.7 eV.[14,15] On the other hand, surface coating NiO such as thin NiO layer formed on yittria-stabilized zirconia was found to show the Ni $2P_{3/2}$ XPS line at 855.9 eV without multiplet splitting peak but with a pronounced satellite at around 862 eV.[16] Similarly, 0.3 wt% NiO-supported SiO_2 sample showed the Ni $2p_{3/2}$ peak at 855.9 eV with a satellite peak at 861.5 eV.[17] Therefore, it can be said that nickel acetate shell coating on the SnO_2 core leads to a thin NiO layer and the appearance of satellite peaks implies the presence of a high-spin

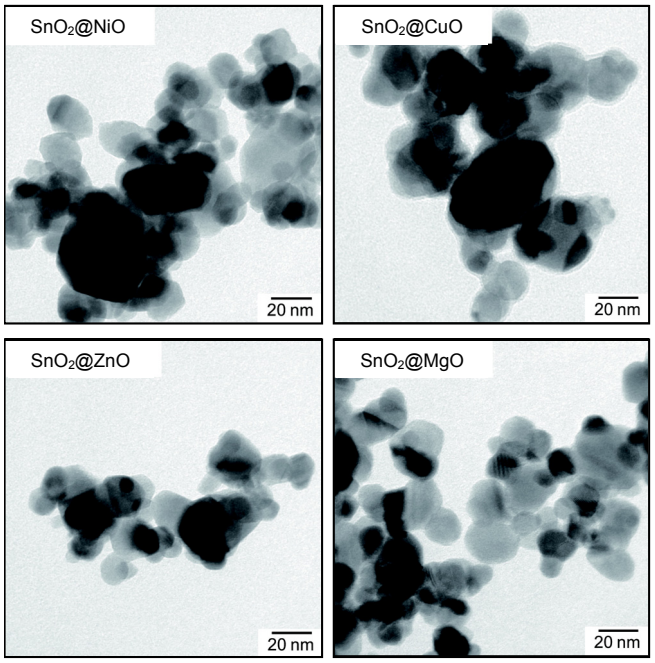

Figure 1. TEM micrographs of the SnO_2 nanoparticle films after shell coatings, where a clear distinction is found for the CuO shell but other shell coatings are hard to be distinguished.

Ni^{2+}.[18] The blue shift in the Ni $2p_{3/2}$ peak position (855.9 eV) and the absence of multiplet splitting peak compared with the XPS characteristics reported for crystalline NiO indicate that the NiO layer formed on the SnO_2 surface has different characteristics from crystalline property. Figure 2(b) shows the Cu 2p XPS spectrum, where the copper acetate treated SnO_2 sample shows a main Cu $2p_{3/2}$ peak at 934.2 eV and broad feature of satellite peak centered at 942.1 eV, which is indicative of Cu^{2+} species with $3d^9$ configuration.[19-21] It was reported that the Cu $2p_{3/2}$ XPS spectrum for the CuO thin amorphous layer of about 5 Å thick on the Cu_2O core material had a main peak at 934.6 eV with a series of satellites on the high-binding-energy side, 940.3 and 943.1 eV.[22] Our XPS result indicates that the surface coating of copper acetate results in CuO layer with Cu^{2+} state. The Zn 2p XPS spectrum (Figure 2(c)) exhibits two main peaks at 1021.7 and 1044.8 eV, which are attributed to $2p_{3/2}$ and $2p_{1/2}$, respectively. The peak positions are in good agreement with the reported literature values for ZnO and the single intense Zn $2p_{3/2}$ feature indicates the presence of only the divalent Zn(II) oxidation state.[23,24] The observed spin-orbit splitting of 23.1 eV is also in good accord with the literature value of 22.97 eV for ZnO.[25] The similar observations were reported for the ZnO-coated TiO_2 nanotube[26] and the core-shell Au@ZnO material.[27] The Mg 1s XPS spectrum (Figure 2(d)) for the magnesium ace-

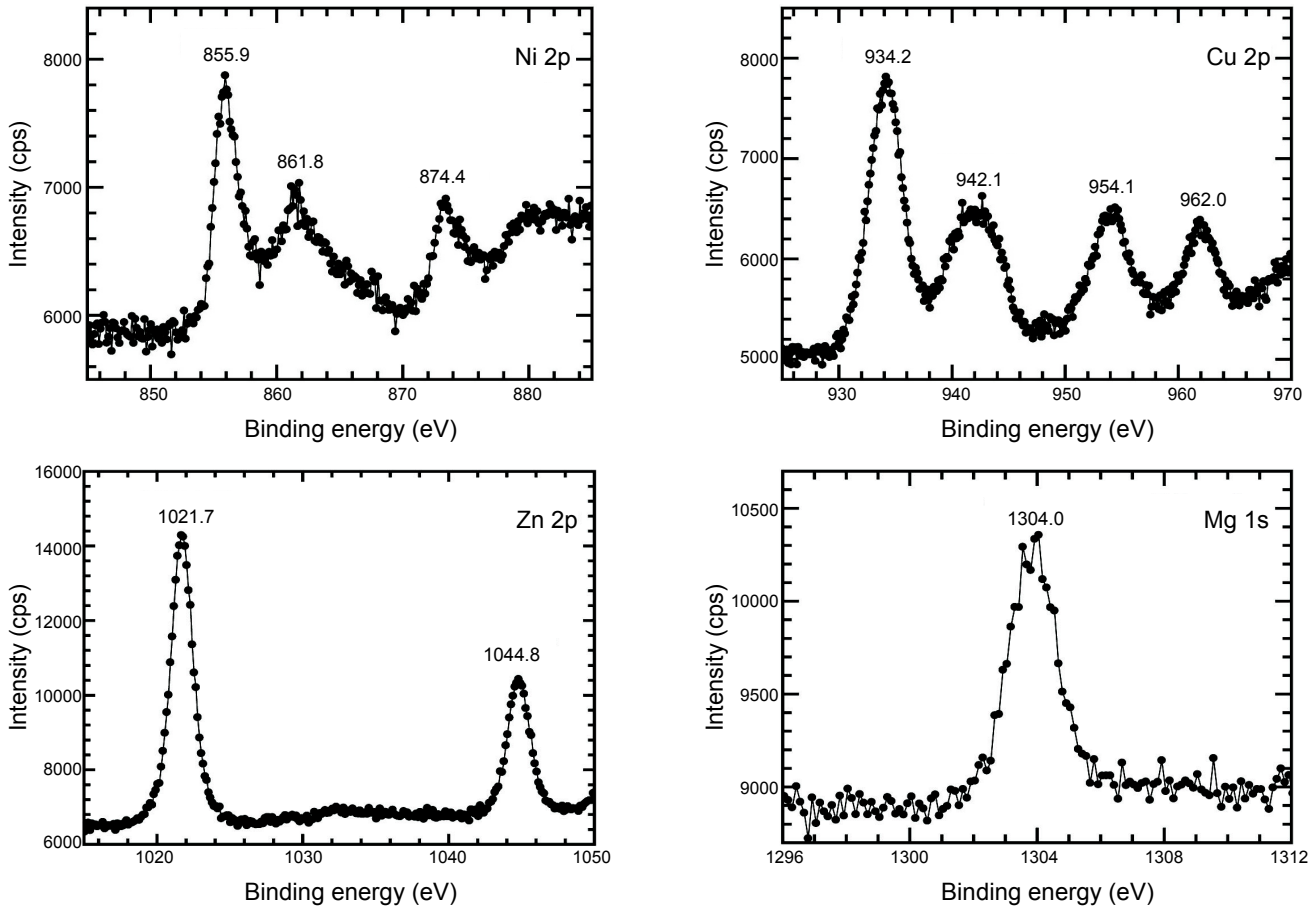

Figure 2. Ni 2p, Cu 2p, Zn 2p and Mg 1s XPS spectra for the SnO_2 nanoparticles treated with Ni, Cu, Zn and Mg acetates. The binding energy in each spectrum was calibrated with C 1s line of 284.8 eV.

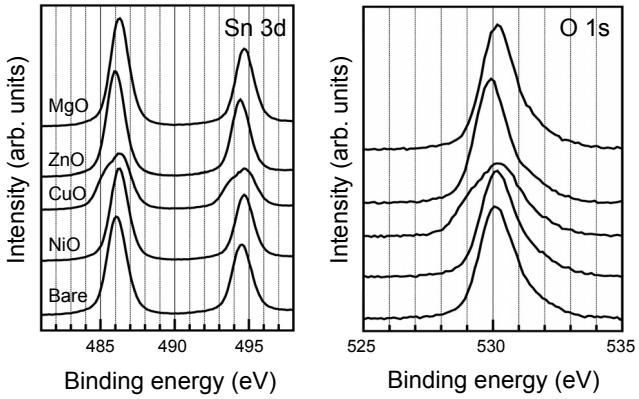

Figure 3. Sn 3d and O 1s XPS spectra of the bare SnO_2 and its surface modified materials. The binding energy in each spectrum was calibrated with C 1s line of 284.8 eV.

tate treated SnO_2 sample shows a single peak at 1304 eV. Corneille *et al.* reported that ultra-thin MgO film with a few angstroms on Mo substrate had Mg 1s line at 1303.6 eV that shifted to lower bind energy when the MgO layer thickness increased due to development of three-dimensional overlayer.[28] Thus, from the combined XPS and TEM analyses, it is expected that magnesium acetate coating leads to ultra-thin and lower dimensional MgO layer on the SnO_2 surface.

Figure 3 compares Sn 3d and O 1s XPS spectra before and after shell coatings. The Sn 3d XPS spectrum for the bare SnO_2 exhibits two peaks at 486.1 eV and 494.6 eV, corresponding to $3d_{5/2}$ and $3d_{3/2}$. Almost no change in binding energies of Sn 3d doublet is observed after shell coatings, which indicates that Sn^{4+} ions in the core material are hardly influenced by shell coatings. For the case of CuO-coated SnO_2 sample, the broad feature appears with shoulder at lower binding energy side. This is presumed to arise from the increased covalent character of Sn^{4+}-O bond due to the introduction of relatively strong ionic character of Cu^{2+}-O bond. Concerning the O 1s XPS spectra, it was reported that the binding energies ranging from 527.7 to 530.6 eV were associated with O^{2-} species, OH^- species appeared from 530.6 to 531.1 eV and the species with the binding energies from 531.1 to 532 eV were described as O^- ions.[29] The O 1s peak for bare SnO_2 shows a slightly asymmetric shape centered at 530 eV, which is therefore assigned to be mostly O^{2-} anions and presence of OH^- ions from higher binding energy side. The O 1s spectral shape and main peak position after shell coatings are almost identical with those for the bare SnO_2, which indicates that surface coatings have little influence on the chemical environment of core material. The broad shape observed for the CuO-coated SnO_2 sample is presumably associated with relatively thick CuO layer as observed in TEM and the shoulder peak at lower binding energy side is therefore related to O^{2-} in CuO.

Photocurrent-voltage characteristics are compared before and after shell coatings in Figure 4(a) and Table 1. Shell coatings result in decrease in photocurrent and increase in photovoltage regardless of the coated materials. The photovoltage of 0.315 V for the bare SnO_2 is substantially improved to about 0.46 V and about 0.6 V after CuO and MgO coatings and NiO and ZnO coatings on its surface, respectively, corresponding to about 46% and 90% increases. Except for the MgO coating, other coatings

Table 1. Photocurrent density (J_{SC}), Voltage (V_{OC}), fill factor (*FF*) and efficiency (η) of dye-sensitized solar cells based on bare SnO_2 and core-shell SnO_2@AO (A = Ni, Cu, Zn and Mg) nanoparticulate films

Samples	J_{SC} (mA/cm^2)	V_{OC} (V)	*FF*	η (%)	Area (cm^2)	Thickness (μm)
Bare SnO_2	9.10	0.315	0.47	1.33	0.254	6.38
SnO_2@NiO	3.91	0.598	0.52	1.21	0.247	6.28
SnO_2@CuO	0.87	0.475	0.70	0.29	0.260	6.22
SnO_2@ZnO	6.49	0.597	0.62	2.40	0.250	6.14
SnO_2@MgO	8.81	0.447	0.52	2.03	0.243	6.19

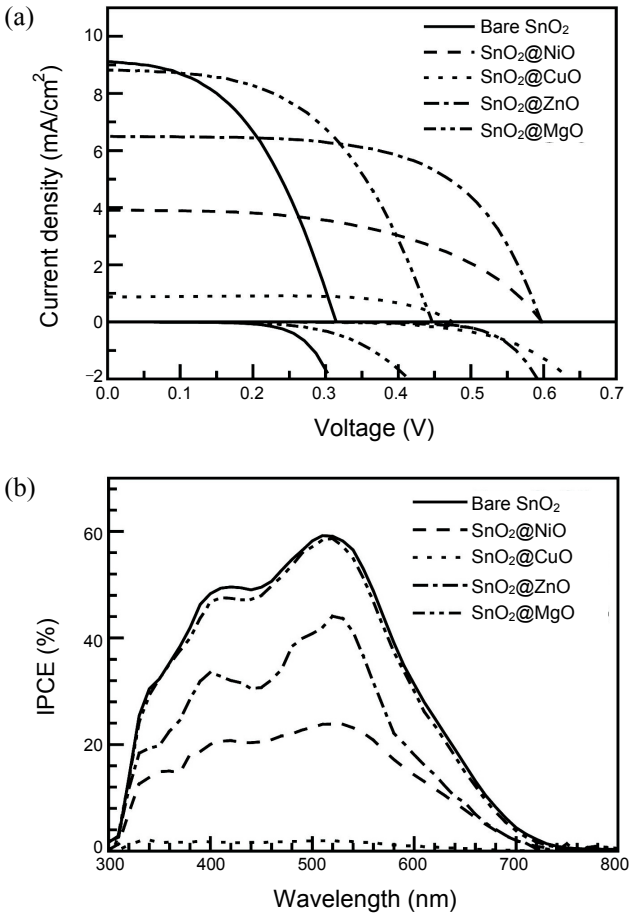

Figure 4. (a) Photocurrent-voltage and dark current-voltage curves and (b) IPCE spectra for the bare SnO_2 and its surface modified materials.

lead to decrease in photocurrent density and the significantly decreased photocurrent after CuO coating is attributed to relatively thick CuO later formed on the SnO_2 surface, associated with difficulty in charge injection. The IPCE spectra in Figure 4(b) show the same tendency observed in the measured photocurrent density under white light. The onset of dark current shifts to higher voltage after shell coatings, which implies that the shell coating protect efficiently the charge transfer from SnO_2 to electrolyte. The reduced dark current correlates with the improvement of photovoltage. From the photocurrent-voltage investigation, it is pointed out that photovoltage is commonly improved regardless of the used shell materials although they

Table 2. Comparison of adsorbed dye amount of bare SnO_2 and core-shell SnO_2@AO (A = Ni, Cu, Zn and Mg) nanoparticulate films

Samples	Amount of dye ($\times 10^{-7}$ mol/cm^2)	Ratio (core-shell/bare)	Area (cm^2)	Thickness (mm)
Bare SnO_2	0.94	1	0.455	6.29
SnO_2@NiO	1.73	1.9	0.450	5.47
SnO_2@CuO	4.81	5.1	0.469	6.33
SnO_2@ZnO	1.79	1.9	0.489	5.66
SnO_2@MgO	1.0	1.1	0.455	6.29

have different conduction band edges.

Figure 5 shows the UV-vis spectra of the solution of dye desorbed to measure the adsorbed dye amount. The estimated absorbed dye is listed in Table 2, where the core-shell materials exhibit higher dye adsorption than the bare SnO_2. Since the isoelectric points of shell materials are higher than that of SnO_2,[30-32] indicating that the surface of the coated SnO_2 is more basic than SnO_2, the higher basicity of the coated surface favors dye attachment through its carboxylic acid groups. Although the shell coatings induce more dye adsorption, photocurrent is not improved, which implies that amount of adsorbed dye does not have direct correlation with the change in photocurrent at least in our core-shell type experiments. Relative thick CuO shell layer is found to have 5 times more dye than the bare SnO_2. However, it shows lowest photocurrent density, which indicates that shell layer may protect charge injection from dye to SnO_2 if it exceeds certain layer thickness.

Electron transport and recombination are investigated in order to understand the basis for the effect of shell coatings. Figure 6 compares the electron diffusion coefficients (D_e), that are obtained from the time constant for electron transport, and the time constants for charge recombination (τ_R) at open-circuit condition before and after shell coatings. Electron diffusion rate decreases after shell coatings as can be seen in Figure 6(a). The decreased photocurrent density is likely to be in part related to the retard transport rate, associated with charge collection efficiency. The slowest rate is observed for the case of CuO shell coating, which is due to rather thick CuO layer compared with thicknesses of other shell materials. This indicates that the electron transport in core-shell structure depends on the thickness of the coated materials. Contrary to the electron transport behavior, time constant for recombination increases after shell coatings compared with the bare SnO_2, which contributes to improvement of photovoltage. Both results suggest that the surface layer and/or the interface between the shell and the core materials act as a barrier in both cases of electron transport through SnO_2 network and electron recombination from SnO_2 to dye.

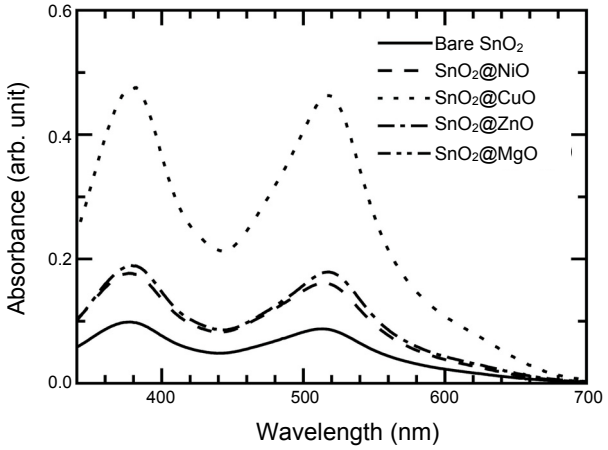

Figure 5. UV-vis spectra of the desorbed N719 dye solution for the bare SnO_2 and its surface modified materials.

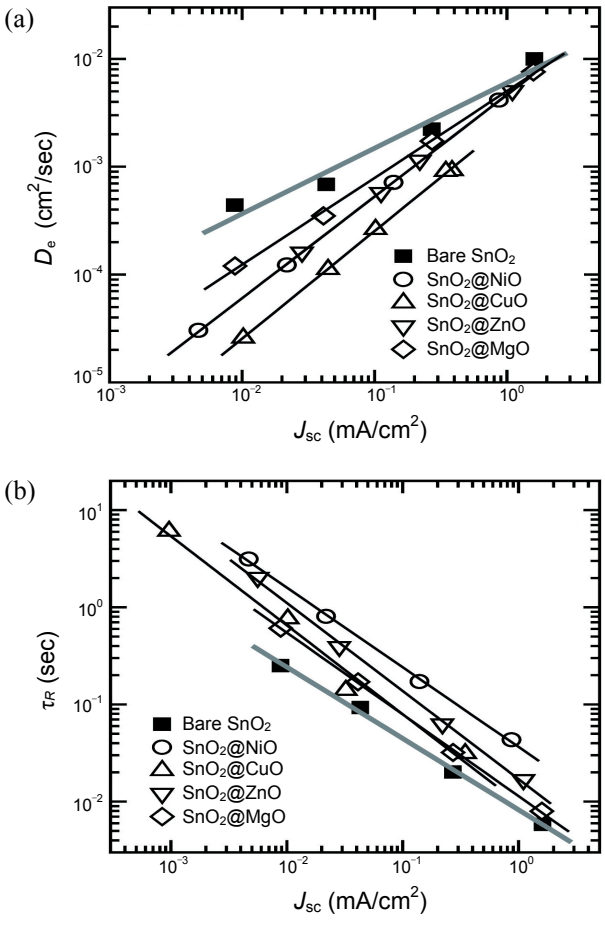

Figure 6. (a) Photocurrent transient spectra and (b) photovoltage transient spectra as a function of light intensity, represented by photocurrent density, for the bare SnO_2 and its surface modified materials.

Conclusion

We have prepared the core-shell materials to investigate the effect of shell coating in dye-sensitized solar cells, where the materials for shell layer have different conduction band edges with respect to the core SnO_2. Shell coatings on the SnO_2 nanocrystalline film resulted commonly in improvement of photovoltage. From the transient photocurrent-voltage spectroscopic studies on the core-shell materials, it was found that charge recombination rate slowed after shell coatings, which was responsible for the improved open-circuit voltage.

Acknowledgments. This work was supported by the National

Research Foundation of Korea (NRF) grant funded by the Ministry of Education, Science and Technology (MEST) of Korea under contracts No. 2009-0092950 and No. 2010-0001842 (ERC program). W. Kang acknowledges the financial support from Seoul R&D program (10543).

References

1. Wang, Q.; Ito, S.; Grätzel, M.; Fabregat-Santiago, F.; Mora-Seró, I.; Bisquert, J.; Bessho, T.; Imai, H. *J. Phys. Chem. B* **2006**, *110*, 25210.
2. Chiba, Y.; Islam, A.; Watanabe, Y.; Komiya, R.; Koide, N.; Han, L. *Jpn. J. Appl. Phys., Pt. 2* **2006**, *45*, L638.
3. Park, N.-G.; Kim, K. *Phys. Stat. Sol. (a)* **2008**, *205*, 1895.
4. Kay, A.; Grätzel, M. *Chem. Mater.* **2002**, *14*, 2930.
5. Park, N.-G.; Kang, M. G.; Kim, K. M.; Ryu, K. S.; Chang, S. H.; Kim, D.-K.; van de Lagemaat, J.; Benkstein, K. D.; Frank, A. J. *Langmuir* **2004**, *20*, 4246.
6. Chappel, S.; Chen, S.-G.; Zaban, A. *Langmuir* **2002**, *18*, 3336.
7. Diamant, Y.; Chen, S. G.; Melamed, O.; Zaban, A. *J. Phys. Chem. B* **2003**, *107*, 1977.
8. Diamant, Y.; Chappel, S.; Chen, S.-G.; Melamed, O.; Zaban, A. *Coord. Chem. Rev.* **2004**, *248*, 1271.
9. Bandaranayake, K. M .P.; Indika Senevirathna, M. K.; Prasad Weligamuwa, P. M. G. M.; Tennakone, K. *Coord. Chem. Rev.* **2004**, *248*, 1277.
10. Ito, S.; Nazeeruddin, K.; Liska, P.; Comte, P.; Charvet, R.; Péchy, P.; Jirousek, M.; Kay, A.; Zakeeruddin, S. M.; Grätzel, M. *Prog. Photovolt: Res. Appl.* **2006**, *14*, 589.
11. Park, J.; Koo, H.-J.; Yoo, B.; Yoo, K.; Kim, K.; Choi, W.; Park, N.-G. *Sol. Energy Mater. Sol. Cells* **2007**, *91*, 1749.
12. Kopidakis, N.; Benkstein, K. D.; van de Lagemaat, J.; Frank, A. J. *J. Phys. Chem. B* **2003**, *107*, 11307.
13. Benkstein, K. D.; Kopidakis, N.; van de Lagemaat, J.; Frank, A. J. *J. Phys. Chem. B* **2003**, *107*, 7759.
14. McIntyre, N. S.; Cook, M. G. *Anal. Chem.* **1975**, *47*, 2208.
15. Roberts, M. W.; Smart, R. St. C. *Surf. Sci.* **1980**, *100*, 590.
16. Khyzhun, O.; Sygellou, L.; Ladas, S. *J. Phys. Chem. B* **2005**, *109*, 2302.
17. Vasilkov, A. Y.; Nikolaev, S. A.; Smirnov, V. V.; Naumkin, A. V.; Volkov, I. O.; Podshibikhin, V. L. *Mendeleev Commun.* **2007**, *17*, 268.
18. Liu, X. F.; Yu, R. H. *J. Appl. Phys.* **2007**, *102*, 083917.
19. Chusuei, C. C.; Brookshier, M. A.; Goodman, D. W. *Langmuir* **1999**, *15*, 2806.
20. Ghijsen, J.; Tjeng, L. H.; Elp, J. V.; Eskes, H.; Westerink, J.; Sawatzky, G. A.; Czyzyk, M. T. *Phys. Rev. B* **1988**, *38*, 11322.
21. Bechara, R.; Aboukais, A.; Bonnelle, J.-P. *J. Chem. Soc. Faraday Trans.* **1993**, *89*, 1257.
22. Yin, M.; Wu, C.-K.; Lou, Y.; Burda, C.; Koberstein, J. T.; Zhu, Y.; O'Brien, S. J. *J. Am. Chem. Soc.* **2005**, *127*, 9506.
23. Puchert, M. K.; Timbrell, P. Y.; Lamb, R. N. *J. Vac. Sci. Technol. A* **1996**, *14*, 2220.
24. Bar, M.; Reichardt, J.; Sieber, I.; Grimm, A.; Kotschau, I.; Lauermann, I.; Sokoll, S.; Lux-Steiner, M. C.; Fischer, C. H.; Niesen, T. P. *J. Appl. Phys.* **2006**, *100*, 23710.
25. Moulder, J. F.; Stickle, W. F.; Sobol, P. E.; Bomben, K. D. *Handbook of X-ray Photoelectron Spectroscopy*; Chastain, J., Ed.; Perkin-Elmer Corporation: USA, Waltham, MA, 1992.
26. Kang, S. H.; Kim, J.-Y.; Kim, Y.; Kim, H. S.; Sung, Y.-E. *J. Phys. Chem. C* **2007**, *111*, 9614.
27. Sun, L.; Wei, G.; Song, Y.; Liu, Z.; Wang, L.; Li, Z. *Mater. Lett.* **2006**, *60*, 1291.
28. Corneille, J. S.; He, J.-W.; Goodman, D. W. *Surf. Sci.* **1994**, *306*, 269.
29. Dupin, J.-C.; Gonbeau, D.; Vinatier, P.; Levasseur, A. *Phys. Chem. Chem. Phys.* **2000**, *2*, 1319.
30. Kosmulski, M. *Chemical Properties of Material Surfaces*; Marcel Dekker: 2001.
31. Lewis, J. A. *J. Am. Ceram. Soc.* **2000**, *83*, 2341.
32. Brunelle, J. P. *Pure Appl. Chem.* **1978**, *50*, 1211.